Nanoscale Research Letters

NANO EXPRESS

Open Access

A Biaxial Strain Sensor Using a Single MoS_2 Grating

Junxiang Xiang[1†], Wenhui Wang[2†], Lantian Feng[3†], Chao Feng[1,4], Meng Huang[1], Ping Liu[1], XiFeng Ren[3*] and Bin Xiang[1*]

Abstract

In this paper, we report a new type of MoS_2-based grating sensor for in-plane biaxial strain gauges with a precision limit of ~ 1‰. The MoS_2 grating is numerically simulated with different biaxial strains up to 5%. Our first-principles calculations reveal that the strain sensitivity of the MoS_2 reflectance spectrum can be considered an additional strain sensor integrated with the grating structure, enabling the mapping of in-plane biaxial strains. Our experimental studies on a prototype MoS_2-grating sensor further confirm that a strain component perpendicular to the grating period can cause intensity peak shifts in the grating's first-order diffraction patterns. This work opens a new path towards the sensing of in-plane biaxial strain within a single-grating device. Our new approach is applicable for other materials that have predictable reflectance response under biaxial strains and the capacity to form a two-dimensional single-crystal layer.

Keywords: Biaxial strain, Grating, Reflectance, MoS_2, First principles

Introduction

Flexible electronics technology has received widespread attention from the academic and industrial communities, but the design and application of microscale and nanoscale flexible devices is challenging due to difficulties in dynamic displacement and deformation monitoring [1–5]. Most conventional strain detection methods based on resistance strain gauges require a miniaturized sensor array [4, 6, 7], which is hard to produce for flexible electronic applications. Optics-based two-dimensional (2D) strain detection techniques, such as speckle interferometry, are superior to those based on piezoresistivity because of their higher precision [8]. However, their image correlation measurement strategy is challenged by the requirements of complex image processing technology [8–10]. A reflection grating can provide a high resolution for the strain measurement but lacks the capability to detect 2D strain within a single device [11].

Over the past years, 2D materials have attracted tremendous research effort. Following the introduction of grapheme [12, 13], the family of 2D materials has been enlarged by many new members such as double atomic thin black phosphorus [14], triple atomic thin transition metal dichalcogenides [15], quadruple atomic thin group-III metal monochalcogenides [16], and other non-layered 2D materials [17]. Many interesting properties have been found in these materials, keeping them under the spotlight of materials science [18–24].

The transition metal dichalcogenides exhibit outstanding optical and mechanical properties [25–27]. For instance, MoS_2 can tolerate as much as 19.5% [26] of biaxial strain accompanied by its reflectance modulation [28], and WSe_2 can show notable Berry curvature dipole as well as nonlinear Hall effect via strain engineering [29]. Incorporating the strain-sensitivity of a material's reflectance spectrum into the function of the reflection

*Correspondence: renxf@ustc.edu.cn; binxiang@ustc.edu.cn
†Junxiang Xiang, Wenhui Wang and Lantian Feng have contributed equally to this work.
[1] Hefei National Research Center for Physical Sciences at the Microscale, Department of Materials Science and Engineering, CAS Key Lab of Materials for Energy Conversion, University of Science and Technology of China, Hefei 230026, Anhui, China
[3] Key Laboratory of Quantum Information, University of Science and Technology of China, Chinese Academy of Sciences, Hefei 230026, China
Full list of author information is available at the end of the article

grating device can be an efficient way to extend strain measurements to biaxial detection within a single device. However, there are no reports of the reflection gratings combined with strain-induced material reflectance modulation for 2D strain sensing applications.

Here, we propose a new type of in-plane biaxial strain sensing technique involving the strain-sensitivity of MoS_2 reflectance in a reflection grating sensor. First-principles calculations reveal that biaxial strains can shift the peak of the intensity distribution in diffraction patterns of a MoS_2-based grating device because the reflectance of MoS_2 is sensitive to the strain-induced deformation. This nonlinear peak shift is well demonstrated by adding a second-order term to the uniaxial-strain linear equation, from which the strain component perpendicular to the grating period direction can be extracted with a precision limit of ~ 1‰. Our experimental studies on a prototype MoS_2-grating device confirm that the strain perpendicular to the grating period can induce an intensity peak shift of the grating's first-order diffraction pattern. Our research shows the possibility of one-shot, in-plane biaxial strain gauges with a single grating sensor.

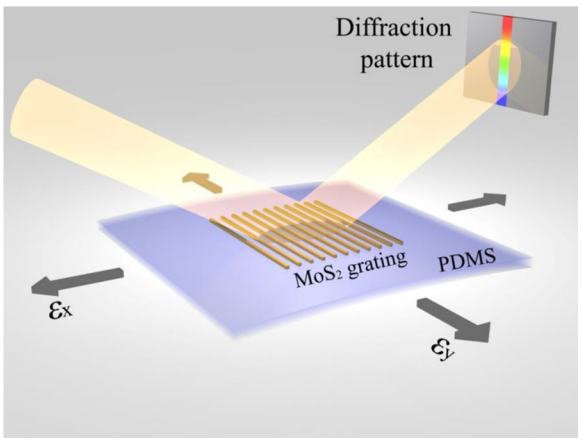

Fig. 1 Schematic illustration of MoS_2-based grating sensor on a flexible substrate of PDMS for biaxial strain gauges

Methods

Theoretical Calculations for MoS_2 Flake

The MoS_2 optical responses to the strain are all studied by first-principle calculations performed with the Vienna Ab-initio Simulation Package (VASP) [30]. All-electron projector augmented wave (PAW) potentials [31] were used for all calculations. Geometric relaxation and static calculations were carried out with the Perdew-Burke-Ernzerhof (PBE) generalized gradient approximation (GGA) method [32]. Spin–orbit coupling (SOC) [33] was also included in the static calculations. To determine the optical properties, quasiparticle energies were first obtained by the GW method derived from Green function theory [34]. The wave function obtained from the static calculations and the quasiparticle energy from the GW calculations were used to perform the Bethe–Salpeter equation (BSE) calculations [35] to predict the dielectric constant.

A bulk crystal model was used to represent the MoS_2 flake (that the optical property differences between stacks greater than five layers is negligible [36]). In the optimization calculations, the energy cutoff was set to 400 eV, and a Monkhorst–Pack k-point set of 15*15*4 was used to sample the Brillouin zone. The lattice parameters were first optimized as a reference for later calculations of the strained MoS_2 flake. The optimized lattice parameters were $a = b = 3.18$ Å and $c = 13.87$ Å. The geometry was relaxed until the energy converged to 10^{-5} eV. Adopting a technique from previous literature [37], an energy cutoff of 300 eV and k-point set of $6 \times 6 \times 2$ were used in the optical calculations. The static energy converged to 10^{-6} eV in all calculations. The diffraction patterns were simulated based on the Helmholtz–Kirchhoff theorem [38]. More details are provided in the Additional file 1.

Preparation of MoS_2 Sample for Spectrum Measurement

The MoS_2 thin film was mechanically exfoliated from a commercial MoS_2 single crystal (SPI Supplies) and transferred to a polydimethylsiloxane (PDMS) substrate with tape. After the transfer, another layer of PDMS was fabricated on the flake and substrate to enhance adhesion.

Preparation of MoS_2 Grating on the Flexible Substrate

The MoS_2 thin film was mechanically exfoliated from a commercial MoS_2 single crystal (SPI Supplies) and transferred to a polydimethylsiloxane (PDMS) substrate with tape. To fabricate the grating device, the MoS_2 flake was firstly patterned into a grating structure by electron beam lithography (EBL). Then the patterned sample was etched by oxygen plasma with a power of 20 W. Finally, we obtained the MoS_2-based grating device by washing away the PMMA.

MoS_2 Device Measurements

A supercontinuum white light source (NKT Photonics SuperK Compact) is used as the excitation laser, which passes through one aperture and hits the flake sample or the grating sample at a certain angle relative to the sample plane, as shown in Fig. 1. In the reflectance measurement, the reflected laser is collected through an optic fiber connected to a spectrometer. The reflectance spectra under different strains are calculated from the data measured by the spectrometer. To test the MoS_2 grating, the reflected laser is projected onto a white board and

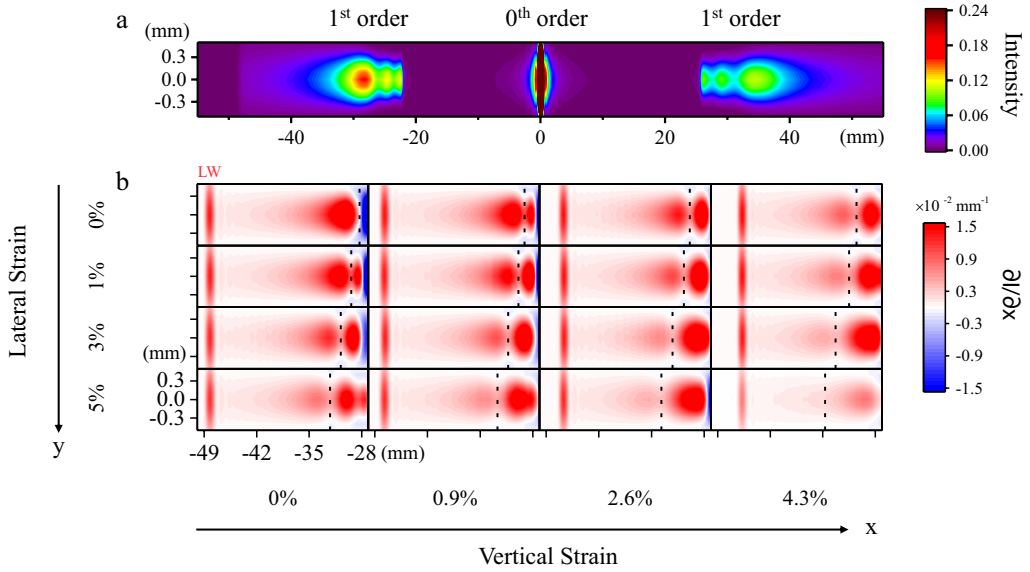

Fig. 2 **a** Simulated image of the diffraction pattern. No strain was applied. The intensity is represented with colors. There is asymmetric behavior between the first-order diffraction spot on both sides of the zero-order beam because the screen in our simulation is set to be parallel to the grating instead of perpendicular to the reflection direction. **b** Simulated evolution of first-order diffraction spot under different biaxial strains. The intensity partial differential is represented with colors. The horizontal coordinate and vertical coordinate denote the position relative to the center of the zero-order diffraction spot. The peak is marked with a dashed line. From left to right, ε_x was set as 0%, 0.9%, 2.6%, and 4.3%, respectively. From top to bottom, the ε_y was 0%, 1%, 3%, and 5%, respectively

appears as a long elliptical light spot. Photos of the light spot are used to analyze the intensity distribution.

Results and Discussion

In a conventional reflection grating sensor, a periodic structure of parallel grating strips can diffract the light, and the diffraction is utilized to measure a strain that is along the grating period direction by monitoring a location shift of the diffraction patterns [11]. Due to the periodic structure orientation, the strain sensing function of the reflection grating is limited to the in-plane uniaxial strain gauge (parallel to the periodic direction). To extend the reflection grating function for use in in-plane biaxial strain gauges, we propose that the intrinsic optical properties of the grating material, such as the strain-sensitivity of the material's reflectance, can be considered as an additional strain sensor to detect in-plane strain components perpendicular to the periodic direction.

MoS_2 has a layered structure: a layer of Mo atoms sandwiched between two layers of S atoms. The interaction between the layers is a weak van der Waals force. Here, we design a MoS_2 flake-based reflection grating sensor (Fig. 1) and investigate the device diffraction patterns under different in-plane biaxial strains by first-principles calculations. The incident beam wavelength range in our calculation is from 400 to 850 nm. The diffraction grating can be described by:

$$d(\sin\theta_{\mathrm{i}} - \sin\theta_{\mathrm{m}}) = n\lambda \tag{1}$$

where d is the distance between two adjacent grating strips, θ_i is the angle between the incident beam and the normal to the grating, θ_m is the angle between the diffraction beam and the normal when the diffraction beam has maxima, n is the diffraction order, and λ is the beam wavelength [11]. From Eq. (1), we see that incident beams with different λ must have different θ_m. Therefore, a continuous wavelength beam causes a continuous series of diffraction spots corresponding to different θ_m, forming an elliptical first-order diffraction pattern.

Figure 2a shows the simulated image of the diffraction patterns of the as-designed grating sensor with no strain applied. Figure 2b shows the intensity peak and pattern location evolution of the simulated first-order diffraction pattern of the device under different biaxial strains. The edge of the first-order diffraction pattern corresponding to the incident beam of 850 nm is labeled "LW". When we apply an in-plane uniaxial tensile strain along the grating period direction (ε_x), this strain can induce an increase in the spacing d between each strip. As a result, θ_m decreases because $d\sin\theta_{\mathrm{m}}$ is constant for any given λ and fixed θ_i. Therefore, when we gradually increase the strain ε_x from 0 to 4.3%, the location of each point in the first-order diffraction pattern moves closer to the center of the zero-order diffraction spot in a proportional relationship

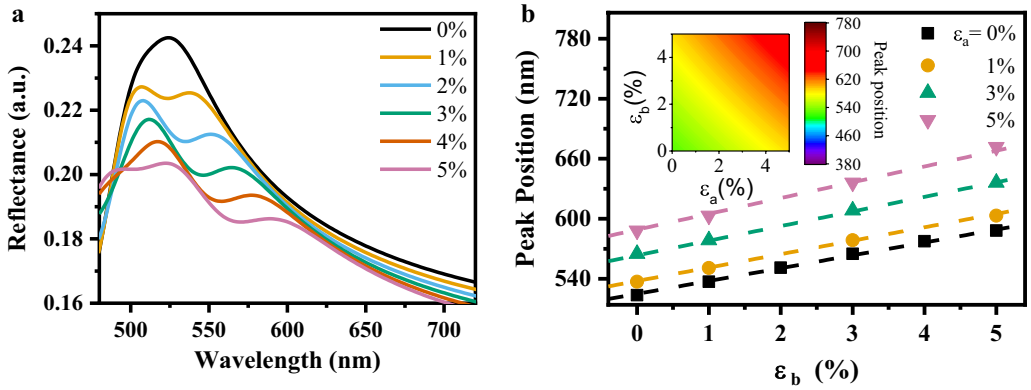

Fig. 3 **a** Reflectance spectra of the MoS_2 flake as a function of wavelength under different uniaxial strains. **b** Peak positions of the reflectance spectra of the MoS_2 flake under different biaxial strains. Dashed lines represent the fitting curves. Inset: The mapping image of peak positions from the fitting equation

with the corresponding beam wavelength, which is consistent with the function of the conventional reflection grating sensor [11].

An incident beam with a longer wavelength λ has a larger θ_m variation, so the LW edge has the most apparent location shift. However, when an in-plane tensile strain perpendicular to the grating period direction (ε_y) is simultaneously applied, an intensity peak shift is observed within the first-order diffraction pattern, as marked by a dashed line in Fig. 2b. When the strain ε_y increases from 0 to 5%, the intensity peak shifts further away from the center of the zero-order diffraction spot. We attribute this peak shift of the intensity distribution to the strain-induced modulation of the MoS_2 reflectance. Previous literature has reported that the reflectance spectrum of MoS_2 can be tuned by an external strain [28], and the reflectance is equal to the intensity ratio of the diffracted beam to the incident beam of the reflection grating. Therefore, the intensity of the beams with different wavelengths diffracted by the MoS_2 grating can be modulated by the in-plane strains. Meanwhile, no LW edge location shift occurs because the strain ε_y exerts no impact on the grating period.

Figure 3a shows the linear behavior in the peak shifts of the MoS_2 reflectance spectra when a uniaxial tensile strain along the lattice vector $\boldsymbol{b}$ of MoS_2 is applied. This uniaxial tensile strain causes a peak-position redshift in the MoS_2 reflectance. However, there is a nonlinear modulation in the reflectance peak position shift when we apply an in-plane biaxial tensile strain. The relationship between the peak position in the reflectance spectra and the in-plane biaxial tensile strain can be described by a second-order equation:

$$\text{Peakposition} = \text{l}(\varepsilon_\text{a} + \varepsilon_\text{b}) + \text{m}\varepsilon_\text{a}\varepsilon_\text{b} + \text{n} \quad (2)$$

where l, m, and n are three constants, and ε_a and ε_b are the strain components along the two lattice vectors of the MoS_2. The first term describes the linear behavior of the peak position shift under uniaxial tensile strains along lattice vector $\boldsymbol{a}$ or $\boldsymbol{b}$. The second term describes the higher-order behavior in the biaxial tensile strain situation. The third term is the reflectance peak position of the unstrained MoS_2. Since the MoS_2 lattice vectors $\boldsymbol{a}$ and $\boldsymbol{b}$ are symmetrically equivalent, the tensile strains along the two directions has the same contribution factor. The fitting results show that the highest difference between the fitting curve and the first-principle-calculated peak positions is 1.76 nm, which indicates that a strain-gauge precision limit of ~ 1‰ can be obtained when the reflectance peak position is utilized to calculate the strain with the Eq. (2). Figure 3b shows the mapping image of the reflectance peak position under different in-plane biaxial tensile strains obtained from the fitted Eq. (2) (see detailed plots of reflectance in Additional file 1).

In our simulation, the lattice vector $\boldsymbol{a}$ is perpendicular to the period direction of the simulated grating. Therefore, the strain ε_y is equal to ε_a, and strain ε_x equals $\sqrt{3}/2 \times \varepsilon_b$. Our calculations reveal that in a MoS_2-based grating sensor, the in-plane strain ε_x can be measured by the LW edge location shift of the first-order diffraction pattern. Based on the intensity peak shift in the first-order diffraction pattern, we can utilize the second-order Eq. (2) to subtract the contribution of the in-plane strain ε_x from the peak shift. Then we can quantitatively calculate the in-plane strain ε_y.

To further experimentally study the strain-sensitivity of the MoS_2 reflectance, we mechanically exfoliated a MoS_2 flake (thickness of several tens of nanometers; see details in Additional file 1) and attached the flake to a flexible substrate of polydimethylsiloxane (PDMS) by

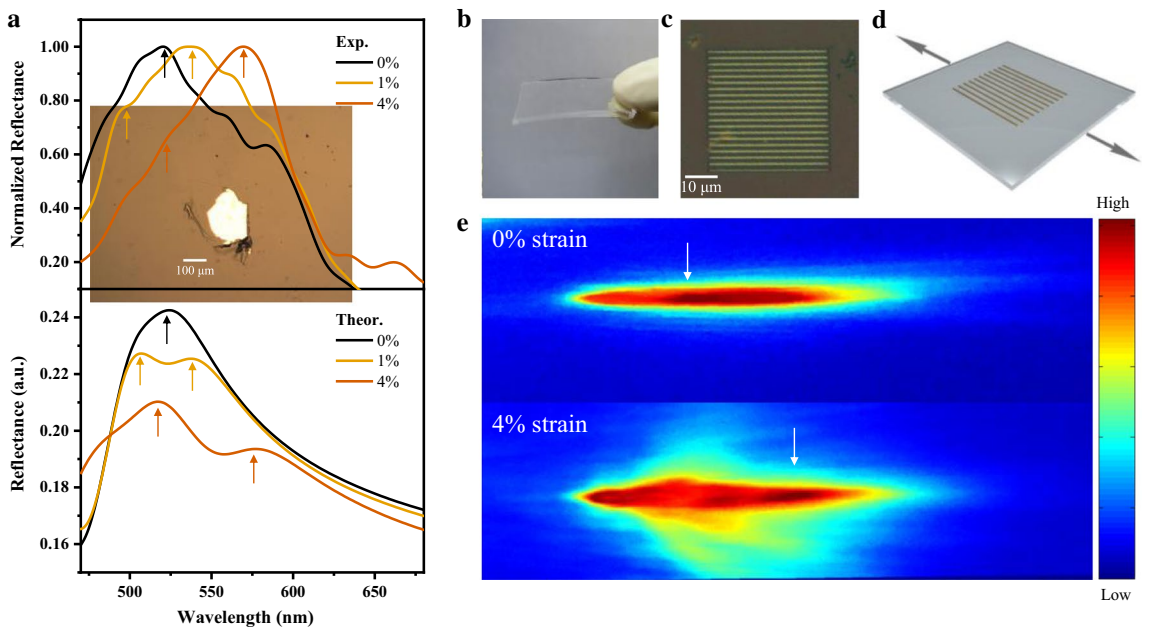

Fig. 4 **a** Experimental results of reflectance spectra with uniaxial strains (top), and the first-principles calculated reflectance spectrum with uniaxial strains (bottom). Arrows indicate the peak locations of the reflectance. Inset, optical image of the MoS_2 flake used for reflectance spectrum testing. **b**–**c** Optical images of the fabricated MoS_2-based grating on PDMS. **d** Schematic diagram of MoS_2-based grating stretched by translation stages. **e** Image of the first-order diffraction spot of the unstrained (top) and the strained (bottom) grating. White arrows indicate the intensity peak

a dry transfer method (shown in Fig. 4a inset). An in-plane uniaxial tensile strain was imposed on this fabricated MoS_2 device by fixing the two sides of the substrate to two translation stages and stretching the substrate. We estimated the in-plane uniaxial tensile strain by calculating $\varepsilon = \delta L/L$, where L is the length of the substrate between the two clips and δL is the length change. When the strain is varied from 0 to 4%, there is a redshift of the peak position in the MoS_2 reflectance spectrum, and the magnitude of this shift agrees well with our theoretical calculations, as shown in Fig. 4a. Figure 4b, c show the optical image of a MoS2-based reflection grating sensor with a period of 2 μm on a PDMS flexible substrate fabricated by electron-beam lithography (details in Methods). Upon stretching the PDMS substrate, an in-plane tensile strain perpendicular to the period direction is exerted on the MoS_2-based grating device (Fig. 4d). By monitoring the intensity distribution in the first-order diffraction pattern, we observed that the intensity peak shifts further away from the center of the zero-order spot compared to the unstrained case when we introduce an in-plane tensile strain of 4% perpendicular to the period direction (Fig. 4e). No diffraction pattern location shift is obtained because the tensile strain is perpendicular to the period direction, and the spacing d between each strip changes little.

Conclusion

In summary, we demonstrate a new technique for gauging in-plane biaxial strain using a MoS_2-based reflection grating sensor. We test the concept by numerically simulating the grating with different biaxial strains up to 5%. In this new technique, the grating structure for detecting the strain component along the period direction (ε_x) is combined with the strain-sensitivity of the MoS_2 reflectance to act as an additional sensor to obtain the in-plane strain component perpendicular to the period direction (ε_y). Component ε_y is calculated with a second-order approximation equation and the intensity peak shift within the first-order diffraction patterns. The theoretical results are well supported by our experiments. Our work opens a path for the design of flexible grating sensors and provides a novel approach to realize one-shot in-plane biaxial strain gauges with a single grating sensor. Our approach is also applicable for other materials that have predictable reflectance response under biaxial strains and the capability to form two-dimensional single-crystal layers.

Supplementary Information

The online version contains supplementary material available at https://doi.org/10.1186/s11671-021-03493-3.

Additional file 1. The supplementary information file contains a detailed description of the numerical simulation method, all results of the dielectric constants and reflectance calculated with different biaxial strains, AFM image of the MoS_2 flake, and Raman spectrum of the MoS_2 grating.

Abbreviations

2D: Two-dimensional; VASP: Vienna Ab-initio Simulation Package; PAW: All-electron projector augmented wave; PBE: Perdew–Burke–Ernzerhof; GGA: Generalized gradient approximation; SOC: Spin–orbit coupling; BSE: Bethe–Salpeter equation; PDMS: Polydimethylsiloxane; EBL: Electron beam lithography.

Acknowledgements

This work was partially carried out at the USTC Center for Micro and Nanoscale Research and Fabrication.

Authors' contributions

JX carried out the whole research and wrote the manuscript. WW supported the simulation. LF supported the optical measurements. CF, MH, and PL supported the device fabrication. XR guided the optical measurements. BX guided all research steps. All authors read and approved the final manuscript.

Funding

National Key Research and Development Program of China (2017YFA0402902).

Availability of data and materials

The datasets used and analyzed during the current study are available from the corresponding author on reasonable request.

Competing interests

The authors declare that they have no competing interests.

Author details

[1] Hefei National Research Center for Physical Sciences at the Microscale, Department of Materials Science and Engineering, CAS Key Lab of Materials for Energy Conversion, University of Science and Technology of China, Hefei 230026, Anhui, China. [2] Research Laboratory for Quantum Materials, Singapore University of Technology and Design, Singapore 487372, Singapore. [3] Key Laboratory of Quantum Information, University of Science and Technology of China, Chinese Academy of Sciences, Hefei 230026, China. [4] Shandong Provincial Key Laboratory of Preparation and Measurement of Building Materials, University of Jinan, Jinan 250022, China.

Received: 23 December 2020 Accepted: 2 February 2021
Published online: 10 February 2021

References

1. Ma YJ, Zhang YC, Cai SS, Han ZY, Liu X, Wang FL, Cao Y, Wang ZH, Li HF, Chen YH, Feng X (2020) Flexible hybrid electronics for digital healthcare. Adv Mater 32:1902062
2. Seyedin S, Zhang P, Naebe M, Qin S, Chen J, Wang XA, Razal JM (2019) Textile strain sensors: a review of the fabrication technologies, performance evaluation and applications. Mater Horiz 6:219–249
3. Lee B, Oh JY, Cho H, Joo CW, Yoon H, Jeong S, Oh E, Byun J, Kim H, Lee S, Seo J, Park CW, Choi S, Park NM, Kang SY, Hwang CS, Ahn SD, Lee JI, Hong Y (2020) Ultraflexible and transparent electroluminescent skin for real-time and super-resolution imaging of pressure distribution. Nat Commun 11:1–11
4. Fu QL, Chen Y, Sorieul M (2020) Wood-based flexible electronics. ACS Nano 14:3528–3538
5. Wang BH, Facchetti A (2019) Mechanically flexible conductors for stretchable and wearable E-skin and E-textile devices. Adv Mater 31:1901408
6. Luo SD, Wang Y, Wang GT, Liu F, Zhai YJ, Luo Y (2018) Hybrid spray-coating, laser-scribing and ink-dispensing of graphene sensors/arrays with tunable piezoresistivity for in situ monitoring of composites. Carbon 139:437–444
7. Wang C, Xu BB, Terry JG, Smith S, Walton AJ, Wang S, Lv HB, Li YF (2019) Flexible, strain gated logic transducer arrays enabled by initializing surface instability on elastic bilayers. APL Mater 7:031509
8. Stetson KA (2018) From the speckle interferometer to digital holography. Proc Spie 10749:107490D
9. Grediac M, Sur F, Blaysat B (2016) The grid method for in-plane displacement and strain measurement: a review and analysis. Strain 52:205–243
10. Pan B, Chen B (2019) A novel mirror-assisted multi-view digital image correlation for dual-surface shape and deformation measurements of sheet samples. Opt Laser Eng 121:512–520
11. Fan B, Dai X, Xie H, Zhao B, Guo B (2017) Dual-light-path optical strain gauge using diffraction grating and position-sensitive detectors for deformation measurement. Exp Mech 57:1275–1287
12. Novoselov KS, Geim AK, Morozov SV, Jiang D, Zhang Y, Dubonos SV, Grigorieva IV, Firsov AA (2004) Electric field effect in atomically thin carbon films. Science 306:666–669
13. Chen ZP, Narita A, Mullen K (2020) Graphene nanoribbons: on-surface synthesis and integration into electronic devices. Adv Mater 32:2001893
14. Li BS, Lai C, Zeng GM, Huang DL, Qin L, Zhang MM, Cheng M, Liu XG, Yi H, Zhou CY, Huang FL, Liu SY, Fu YK (2019) Black phosphorus, a rising star 2D nanomaterial in the post-graphene era: synthesis, properties, modifications, and photocatalysis applications. Small 15:1804565
15. Seol M, Lee MH, Kim H, Shin KW, Cho Y, Jeon I, Jeong M, Lee HI, Park J, Shin HJ (2020) High-throughput growth of wafer-scale monolayer transition metal dichalcogenide via vertical ostwald ripening. Adv Mater 32:2003542
16. D'Olimpio G, Nappini S, Vorokhta M, Lozzi L, Genuzio F, Mentes TO, Paolucci V, Gurbulak B, Duman S, Ottaviano L, Locatelli A, Bondino F, Boukhvalov DW, Politano A (2020) Enhanced electrocatalytic activity in GaSe and InSe nanosheets: the role of surface oxides. Adv Funct Mater 30:2005466
17. Tan CL, Zhang H (2015) Wet-chemical synthesis and applications of non-layer structured two-dimensional nanomaterials. Nat Commun 6:7873
18. Al-Abbas SSA, Muhsin MK, Jappor HR (2019) Two-dimensional GaTe monolayer as a potential gas sensor for SO_2 and NO_2 with discriminate optical properties. Superlattice Microstruct 135:106245
19. Almayyali AOM, Kadhim BB, Jappor HR (2020) Tunable electronic and optical properties of 2D PtS_2/MoS_2 van der Waals heterostructure. Physica E 118:113866
20. Almayyali AOM, Kadhim BB, Jappor HR (2020) Stacking impact on the optical and electronic properties of two-dimensional $MoSe_2/PtS_2$ heterostructures formed by PtS_2 and $MoSe_2$ monolayers. Chem Phys 532:110679
21. Obeid MM, Stampfl C, Bafekry A, Guan Z, Jappor HR, Nguyen CV, Naseri M, Hoat DM, Hieu NN, Krauklis AE, Vu TV, Gogova D (2020) First-principles investigation of nonmetal doped single-layer BiOBr as a potential photocatalyst with a low recombination rate. Phys Chem Chem Phys 22:15354–15364
22. Cai YQ, Zhang G, Zhang YW (2014) Polarity-reversed robust carrier mobility in monolayer MoS_2 nanoribbons. J Am Chem Soc 136:6269–6275
23. Cai YQ, Lan JH, Zhang G, Zhang YW (2014) Lattice vibrational modes and phonon thermal conductivity of monolayer MoS_2. Phys Rev B 89:035438
24. Cai YQ, Ke QQ, Zhang G, Feng YP, Shenoy VB, Zhang YW (2015) Giant phononic anisotropy and unusual anharmonicity of phosphorene: interlayer coupling and strain engineering. Adv Funct Mater 25:2230–2236
25. Zollner K, Faria PE, Fabian J (2019) Strain-tunable orbital, spin-orbit, and optical properties of monolayer transition-metal dichalcogenides. Phys Rev B 100:195126
26. Li TS (2012) Ideal strength and phonon instability in single-layer MoS2. Phys Rev B 85:235407
27. Bertolazzi S, Brivio J, Kis A (2011) Stretching and breaking of ultrathin MoS_2. ACS Nano 5:9703–9709
28. Frisenda R, Druppel M, Schmidt R, de Vasconcellos SM, de Lara DP, Bratschitsch R, Rohlfing M, Castellanos-Gomez A (2017) Biaxial strain tuning of the optical properties of single-layer transition metal dichalcogenides. NPJ 2D Mater Appl 1:1–7

29. Qin M-S, Zhu P-F, Ye X-G, Xu W-Z, Song Z-H, Liang J, Liu K, Liao Z-M (2021) Strain tunable berry curvature dipole, orbital magnetization and nonlinear hall effect in WSe_2 monolayer. Chin Phys Lett 38:017301
30. Kresse G, Furthmuller J (1996) Efficient iterative schemes for ab initio total-energy calculations using a plane-wave basis set. Phys Rev B 54:11169–11186
31. Kresse G, Joubert D (1999) From ultrasoft pseudopotentials to the projector augmented-wave method. Phys Rev B 59:1758–1775
32. Perdew JP, Burke K, Ernzerhof M (1996) Generalized gradient approximation made simple. Phys Rev Lett 77:3865–3868
33. Steiner S, Khmelevskyi S, Marsmann M, Kresse G (2016) Calculation of the magnetic anisotropy with projected-augmented-wave methodology and the case study of disordered $Fe_{1-x}Co_x$ alloys. Phys Rev B 93:6
34. Shishkin M, Kresse G (2006) Implementation and performance of the frequency-dependent GW method within the PAW framework. Phys Rev B 74:035101
35. Albrecht S, Reining L, Del Sole R, Onida G (1998) Ab initio calculation of excitonic effects in the optical spectra of semiconductors. Phys Rev Lett 80:4510–4513
36. Mak KF, Lee C, Hone J, Shan J, Heinz TF (2010) Atomically thin MoS_2: a new direct-gap semiconductor. Phys Rev Lett 105:136805
37. Ramasubramaniam A (2012) Large excitonic effects in monolayers of molybdenum and tungsten dichalcogenides. Phys Rev B 86:115409
38. Born M, Wolf E (1999) Principles of optics: electromagnetic theory of propagation, interference and diffraction of light, 7th edn. Cambridge University Press, Cambridge

Publisher's Note